Geochemistry Geophysics Geosystems G3

Article
Volume 12, Number 6
14 June 2011
Q06003, doi:10.1029/2010GC003412
ISSN: 1525-2027

Published by AGU and the Geochemical Society

Volcanic CO_2 output at the Central American subduction zone inferred from melt inclusions in olivine crystals from mafic tephras

H. Wehrmann
SFB 574 at the University of Kiel, IFM-GEOMAR, Wischhofstr. 1-3, D-24148 Kiel, Germany

K. Hoernle
SFB 574 at the University of Kiel, IFM-GEOMAR, Wischhofstr. 1-3, D-24148 Kiel, Germany

Leibniz Institute of Marine Sciences, IFM-GEOMAR, Wischhofstr. 1-3, D-24148 Kiel, Germany

M. Portnyagin
Leibniz Institute of Marine Sciences, IFM-GEOMAR, Wischhofstr. 1-3, D-24148 Kiel, Germany

V. I. Vernadsky Institute of Geochemistry and Analytical Chemistry, Kosigin st. 19, D-119991 Moscow, Russia

M. Wiedenbeck
Helmholtz Centre Potsdam, GFZ German Research Centre for Geosciences, Telegrafenberg, D-14473 Potsdam, Germany

K. Heydolph
SFB 574 at the University of Kiel, IFM-GEOMAR, Wischhofstr. 1-3, D-24148 Kiel, Germany

Leibniz Institute of Marine Sciences, IFM-GEOMAR, Wischhofstr. 1-3, D-24148 Kiel, Germany

[1] The volatile contents of olivine-hosted (Fo_{89-71}) melt inclusion glasses in rapidly quenched mafic tephras from volcanic front volcanoes of the Central American Volcanic Arc (CAVA) in Guatemala, Nicaragua, and Costa Rica, were analyzed by secondary ion mass spectrometry (SIMS) in order to derive the minimum eruptive output of CO_2, along with H_2O, Cl, and S. Details of the analytical method are provided that establish melt inclusion CO_2 analyses with the Cameca ims6f at the Helmholtz Centre Potsdam. The highest CO_2 concentrations (up to 1800 μg/g) are observed in Nicaraguan samples, while melt inclusions from Guatemala and Costa Rica have CO_2 contents between 50 and 500 μg/g. CO_2 does not positively covary with sediment/slab fluid tracers such as Ba/La, Ba/Th, or U/La. Instead, the highest CO_2 concentrations occur in the inclusions with the most depleted incompatible element compositions and low H_2O, approaching the composition of mid-ocean ridge basalts (MORBs), whereas the most H_2O-rich inclusions are relatively CO_2-poor (<800 μg/g). This suggests that CO_2 degassing was more extensive in the melts with the highest slab contribution. CO_2/Nb ratios in the least degassed CAVA melt inclusions are similar to those of primitive MORBs. These are interpreted here as recording a minimum CO_2 output rate from the mantle wedge, which amounts to 2.8×10^4 g/s for the ~1100 km long CAVA. Previously published estimates from quiescent degassing and numerical modeling, which also encompassed the slab contribution, are 3 times higher. This comparison allows us to estimate the proportion of the total CO_2 output derived from the mantle wedge.

Components: 10,300 words, 9 figures, 1 table.

Keywords: CO_2; Central American Volcanic Arc; melt inclusions; secondary ion mass spectrometry; subduction zone volatile emission rates.

Index Terms: 1031 Geochemistry: Subduction zone processes (3060, 3613, 8170, 8413); 1043 Geochemistry: Fluid and melt inclusion geochemistry; 1094 Geochemistry: Instruments and techniques.

Received 20 October 2010; **Revised** 18 April 2011; **Accepted** 18 April 2011; **Published** 14 June 2011.

Wehrmann, H., K. Hoernle, M. Portnyagin, M. Wiedenbeck, and K. Heydolph (2011), Volcanic CO_2 output at the Central American subduction zone inferred from melt inclusions in olivine crystals from mafic tephras, *Geochem. Geophys. Geosyst.*, *12*, Q06003, doi:10.1029/2010GC003412.

Theme: Central American Subduction System

1. Introduction

[2] Subduction zone volcanoes are significant contributors of gases to the Earth's surface and the atmosphere. Organic materials, sediments and seawater can be transported into the mantle at convergent plate margins, where they induce melting leading to arc volcanism. Volatile phases are returned to the surface by both fluid cycling within the fore arc and volcanic activity in the arc. Of the gas species that may be released from magmatic systems into the atmosphere, CO_2 is considered to be one of the most important elements with regard to long-term global climate evolution.

[3] In the past, several strategies have been employed to understand patterns and quantify natural emissions of CO_2 from subduction zones via studies of quiescent and eruptive degassing of arc volcanoes [e.g., *Hilton et al.*, 2002; *Shaw et al.*, 2003, 2007; *de Leeuw et al.*, 2007], by fore-arc seafloor venting [e.g., *Kulm and Suess*, 1990; *Fryer et al.*, 1999], or by using numerical modeling [e.g., *Connolly*, 2005; *Gorman et al.*, 2006]. This study is focused on the cycling of CO_2 through the Central American subduction zone, where the amounts of subducted carbonate-bearing lithologies and organic-rich hemipelagic sediments are at a global maximum [e.g., *Tera et al.*, 1986; *Carr et al.*, 1990; *Plank et al.*, 2002]. An important question is to what extent such large carbon inputs affect the CO_2 output of the subduction zone. At the Central American Volcanic Arc (CAVA), several studies have determined the volcanic CO_2 emission from hydrothermal vents (i.e., hot springs, fumaroles, wells) [*Snyder et al.*, 2001; *Hilton et al.*, 2002; *Shaw et al.*, 2003; *de Leeuw et al.*, 2007]; and individual volcanoes were investigated for eruptive CO_2 release via melt inclusion analyses (e.g., Fuego [*Roggensack*, 2001a], Cerro Negro [*Roggensack et al.*, 1997; *Roggensack*, 2001b], Irazú [*Benjamin et al.*, 2007], Arenal [*Wade et al.*, 2006]). Variations in melt inclusion CO_2 contents across a Guatemalan arc segment were described by *Walker et al.* [2003].

[4] The major goals of this study are to establish the analysis of CO_2 through secondary ion mass spectrometry (SIMS) on melt inclusions and to determine CO_2 contents in olivine-hosted melt inclusions in mafic tephras from nine volcanoes along the volcanic front in Central America. These data are then used to evaluate whether the CO_2 concentrations reflect magmatic values or are features induced by preentrapment degassing. The inclusions with the most depleted MORB-like compositions are processed to estimate the minimum CO_2 output rate at the CAVA, which, combined with published data for total fluxes, allows us to estimate the proportion of the slab contribution.

2. Geologic Setting

[5] Volcanic activity at the CAVA results from the northeastward subduction of the Cocos Plate beneath the Caribbean Plate (Figure 1), at a convergence rate of ~74–85 mm/yr [*DeMets*, 2001]. The subducting slab outboard of northwest Central America has normal mid-ocean ridge basalt (N-MORB) type composition, while the uppermost mantle of the incoming plate outboard of Nicaragua has been hydrated and converted to serpentinite at the outer rise due to extensive bend-faulting reaching down to mantle depths [*Ranero et al.*, 2003; *Grevemeyer et al.*, 2007; *Ivandic et al.*, 2008]. Younger crust of the Galapagos hot spot track subducts beneath Costa Rica and western Panama [*Werner et al.*, 1999, 2003; *Hoernle et al.*, 2000, 2002, 2008; *Sadofsky et al.*, 2009]. The subduc-

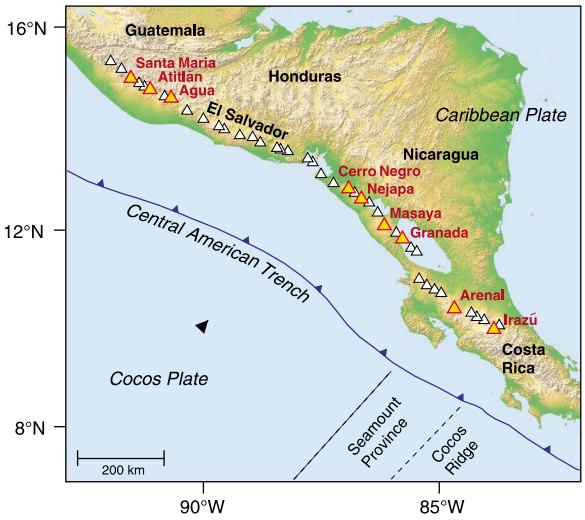

Figure 1. Schematic map of the Central American Volcanic Arc, formed by the subduction of the Cocos Plate beneath the Caribbean Plate. The Galapagos hot spot track (Seamount Province and Cocos Ridge) is subducting beneath Costa Rica. The yellow-red triangles indicate the volcanic front volcanoes, for which we report melt inclusion data in this study; the white triangles indicate other volcanic front volcanoes. Image courtesy SRTM Team NASA/JPL/NIMA, modified.

tion geometry (Figure 2) is characterized by thick (~46 km) continental crust of the overriding plate in northwestern Guatemala, where the slab subducts at an angle of about 48°. From El Salvador to Nicaragua, the slab angle steepens to a maximum of 64° [*Syracuse and Abers*, 2006] and the crust thins to ~25 km beneath the Nicaragua volcanic front [e.g., *Ligorria and Molina*, 1997; *Narcía-López et al.*, 2004; *Auger et al.*, 2006; *MacKenzie et al.*, 2008]. Further south in Costa Rica and Panama, the slab angle becomes shallower again (44°) and the mafic crust thickens to ~38 km [*MacKenzie et al.*, 2008].

3. Methods

[6] Olivine-hosted melt inclusions were selected for analysis from young (Holocene to historic) mafic tephras erupted from volcanoes along the CAVA (Figure 1). These inclusions had been previously analyzed for major elements, sulfur and chlorine by electron microprobe at IFM-GEOMAR using a Cameca SX 50, and for trace elements, water and fluorine with a Cameca ims4f ion microprobe at the Institute of Microelectronics and Informatics, Yaroslavl, Russia [*Sadofsky et al.*, 2008]. All the studied inclusions are glassy and usually contain small gas bubbles; they were not reheated/homogenized prior to analysis. Whole-rock analyses of some of the samples are presented by *Hoernle et al.* [2008] and *Gazel et al.* [2009].

[7] CO_2, H_2O, Cl, and S concentrations presented in this paper were determined using a Cameca ims6f ion microprobe at the Helmholtz Centre Potsdam. For the purpose of interlaboratory comparison and also to confirm the external repeatability of the data, the Cl and S contents in the melt inclusions were replicated (comparative plots are provided in Figure S1 in the auxiliary material).[1] The polished and ethanol-cleaned olivine crystals were mounted together with the reference materials in indium metal contained on a single aluminum disk (adopting the procedure of *Hauri et al.* [2002] and *Koga et al.* [2003] and stored for two months in an ultrahigh vacuum before being inserted into the instrument. The strict avoidance of epoxy has proved crucial to minimize background values by preventing degradation of vacuum in the secondary ion source chamber, which remained stable at ~2×10^{-10} torr throughout the measurement series. A primary voltage of 10 kV was applied to the primary $^{133}Cs^+$ source, and an electron flood gun operated at ~5 μA was used to achieve charge compensation. To eliminate isobaric molecular interferences, a mass resolving power of M/dM = 3500 was applied. For the analyses, the beam was set to raster an area of 40 μm, in conjunction with an 8 μm field-of-view aperture so as to ensure that no contaminants from the margins of the rastered area reached the detector.

[8] The Cameca ims6f ion microprobe was calibrated using a set of natural basaltic and andesitic glasses: Na22-5, ALV519-4, CFA-47, Na23-6, A-46, TRD 80, SC1, OB93, 169ds2, P2-3, P103-2, 30-2, 40-2, Etna 2, and Etna 3 [*Sobolev and Chaussidon*, 1996; *Dixon*, 1997; *Danyushevsky et al.*, 2000] (and unpublished data kindly provided by R. Botcharnikov, Hannover, 2008). To quantify the volatile element concentrations, intensities of the secondary ions $^1H^-$, $^{12}C^-$, $^{32}S^-$, $^{35}Cl^-$ were measured and normalized to the intensity of $^{28}Si^-$. The data obtained on the reference glasses are presented in Table S1 in the auxiliary material and are used to constrain calibration curves presented in Figure 3. The two main reference materials (Na22-5, ALV519-4) were measured two to three times per day during the 5 day analytical run and proved highly reproducible with a repeatability of 5.3% (Na22-5, 1σ, N = 10) and 6.2% (ALV519-4, 1σ, N = 9) relative for CO_2. The other reference

[1] Auxiliary materials are available in the HTML. doi:10.1029/2010GC003412.

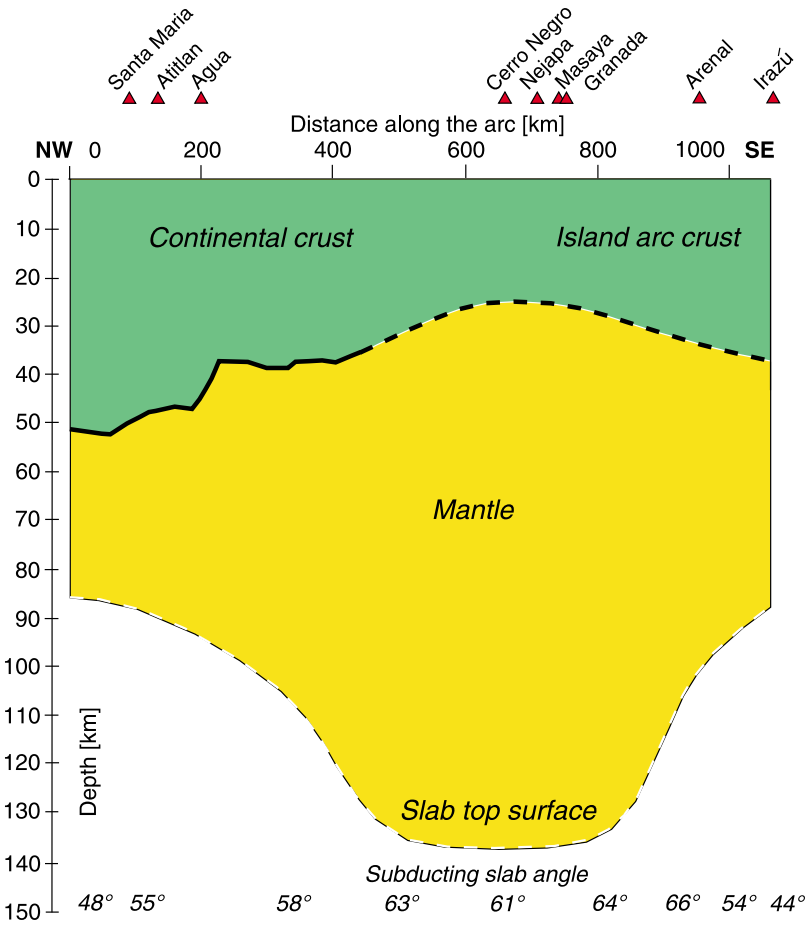

Figure 2. Along-arc profile of the CAVA, extending ~1000 km, illustrating the variations in the depth to the surface of the subducting slab, crustal thickness, mantle wedge thickness and composition of the overlying crust. The crust is thinnest beneath Nicaragua and thickens both to the north toward Guatemala and to the south toward Costa Rica. Slab depth and Guatemalan crustal thickness from *Syracuse and Abers* [2006]; crustal thicknesses of Nicaragua and Costa Rica from *MacKenzie et al.* [2008].

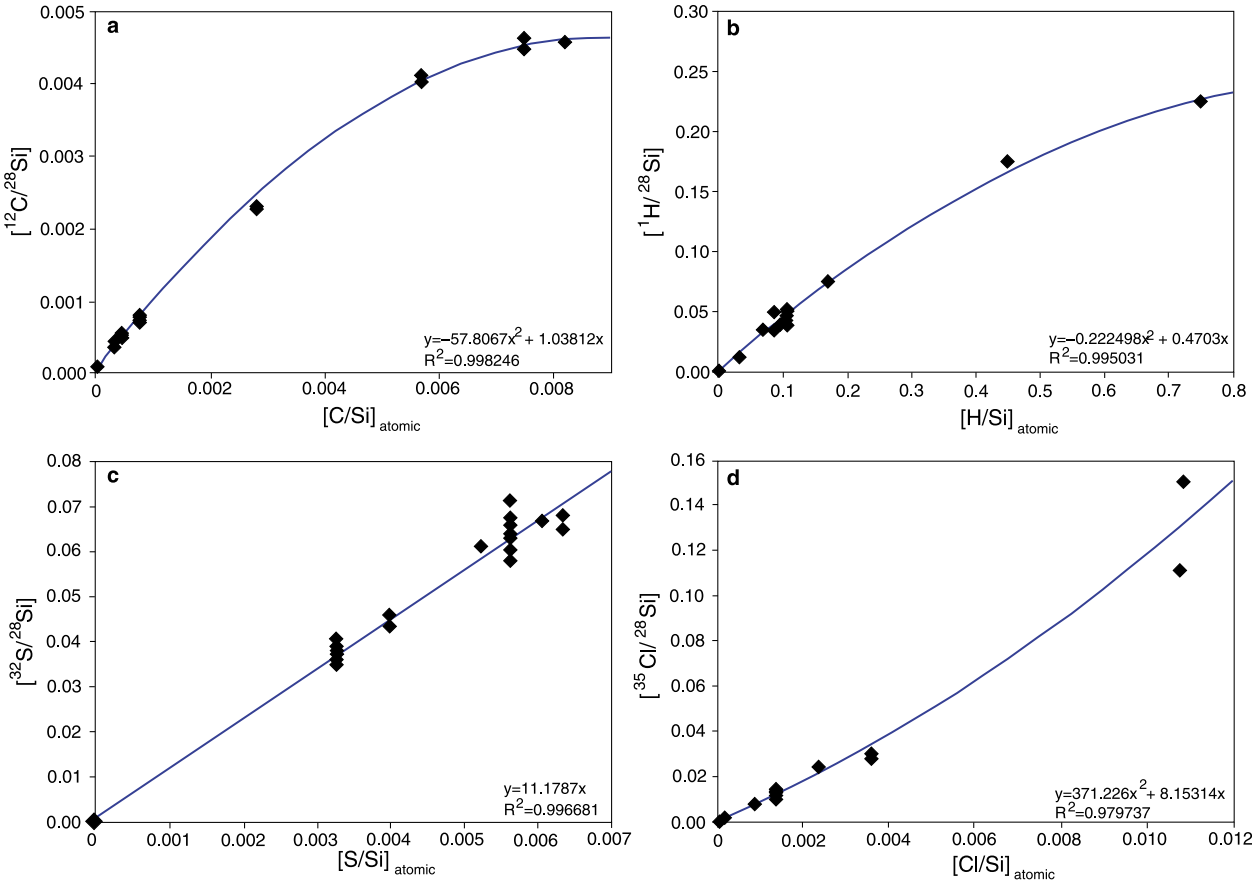

Figure 3. SIMS calibration curves for abundances of (a) carbon dioxide, (b) water, (c) sulfur and (d) chlorine.

Table 1 (Sample). Compositions of Melt Inclusions in Olivine From the Central American Volcanic Arc[a] [The full Table 1 is available in the HTML version of this article]

Volcano	Segment	Rock Sample	Inclusion	H_2O	CO_2	S	Cl	F	SiO2
Analytical method				SIMS	SIMS	SIMS	SIMS	SIMS	EMP
Santa María	GU	GU19d	1b	1.50	486	1380	572	519	53.07
Santa María	GU	GU19d	3a	2.23	214	1224	817	n.d.	56.19
Santa María	GU	GU19d	3b	2.24	273	1195	746	n.d.	56.61
Santa María	GU	GU19d	6	2.69	165	1931	990	n.d.	53.35
Atitlán	GU	GU25b	1	2.34	461	1690	1192	414	54.97
Atitlán	GU	GU25b	3	2.47	94	988	1051	456	55.23
Agua	GU	GU11d	2a	2.77	300	2303	1481	661	53.82
Agua	GU	GU11d	2b	2.65	n.d.	1081	1915	n.d.	55.30
Agua	GU	GU11d	1	1.77	304	2611	1329	296	51.93
Cerro Negro	NWN	P2-3a	2-46a	2.81	464	1862	1277	122	49.53
Cerro Negro	NWN	P2-3a	46b	3.11	409	1477	1007	n.d.	50.01
Cerro Negro	NWN	P2-3a	3-10	4.99	755	1584	926	144	50.35
Cerro Negro	NWN	P2-3b	2-60a	2.34	210	1422	1266	n.d.	48.91
Cerro Negro	NWN	P2-3b	2-60b	0.75	68	1065	1418	n.d.	50.22
Cerro Negro	NWN	P2-3d	1a	2.29	155	546	965	219	53.16
Cerro Negro	NWN	P2-3d	1b	2.66	435	1679	1033	n.d.	47.90
Nejapa	SEN	P2-32d	1	0.51	85	242	460	255	50.32
Nejapa	SEN	P2-32d	2	1.19	140	853	453	202	48.65
Nejapa	SEN	P2-32d	3a	1.84	n.d.	1058	299	119	47.80
Nejapa	SEN	P2-32d	3b	1.65	1543	1129	320	n.d.	48.90
Nejapa	SEN	P2-32d	4a	1.63	1466	1685	659	291	47.26
Nejapa	SEN	P2-32d	4b	1.84	1419	1221	325	171	47.68
Nejapa	SEN	P2-32d	6a	1.55	1777	1193	316	100	48.74
Nejapa	SEN	P2-32d	6b	1.50	n.d.	1281	405	n.d.	48.92
Nejapa	SEN	P2-32d	7	0.76	83	1089	462	351	48.54
Masaya	SEN	P2-47	2	1.39	369	448	1278	475	52.60
Masaya	SEN	P2-47	3a	1.91	n.d.	420	1531	597	53.71
Masaya	SEN	P2-47	3b	1.47	n.d.	365	1382	672	53.37
Granada	SEN	P2-58	27a	3.22	281	1037	1414	186	52.20
Granada	SEN	P2-58	27b	3.34	93	1721	839	139	50.89
Granada	SEN	P2-58	8	2.73	n.d.	2047	1081	203	47.57
Granada	SEN	P2-58	2-07	2.04	692	2219	906	131	46.54
Granada	SEN	P2-58	2-59	1.97	1451	1301	591	172	47.93
Granada	SEN	P2-58	2-32	1.94	1200	1346	557	160	49.42
Arenal	CR	CR-61C	53	1.03	136	2065	1655	407	50.68
Arenal	CR	CR-61C	57	1.16	346	1814	1742	350	50.94
Arenal	CR	CR-61C	59	1.42	131	2033	2069	n.d.	51.40
Irazú	CR	P2-72	40a	0.81	147	222	2287	2143	60.43
Irazú	CR	P2-72	40b	0.78	445	293	3137	3159	57.62
Irazú	CR	P2-72	10	1.51	n.d.	475	3704	2633	63.29
Irazú	CR	P2-72	3-01	3.01	194	2009	751	611	52.33
Irazú	CR	P2-72	3-02	2.11	56	1388	877	712	52.05

[a]Volatile concentrations except F from this study (H_2O in wt %, CO_2, S, Cl in μg/g; corrected for postentrapment crystallization); major elements (wt %), F (μg/g) and nonvolatile trace elements (μg/g) and host olivine compositions (wt %) from *Sadofsky et al.* [2008]. Major elements normalised to 100% volatile free. Original total retained; n.d., not determined.

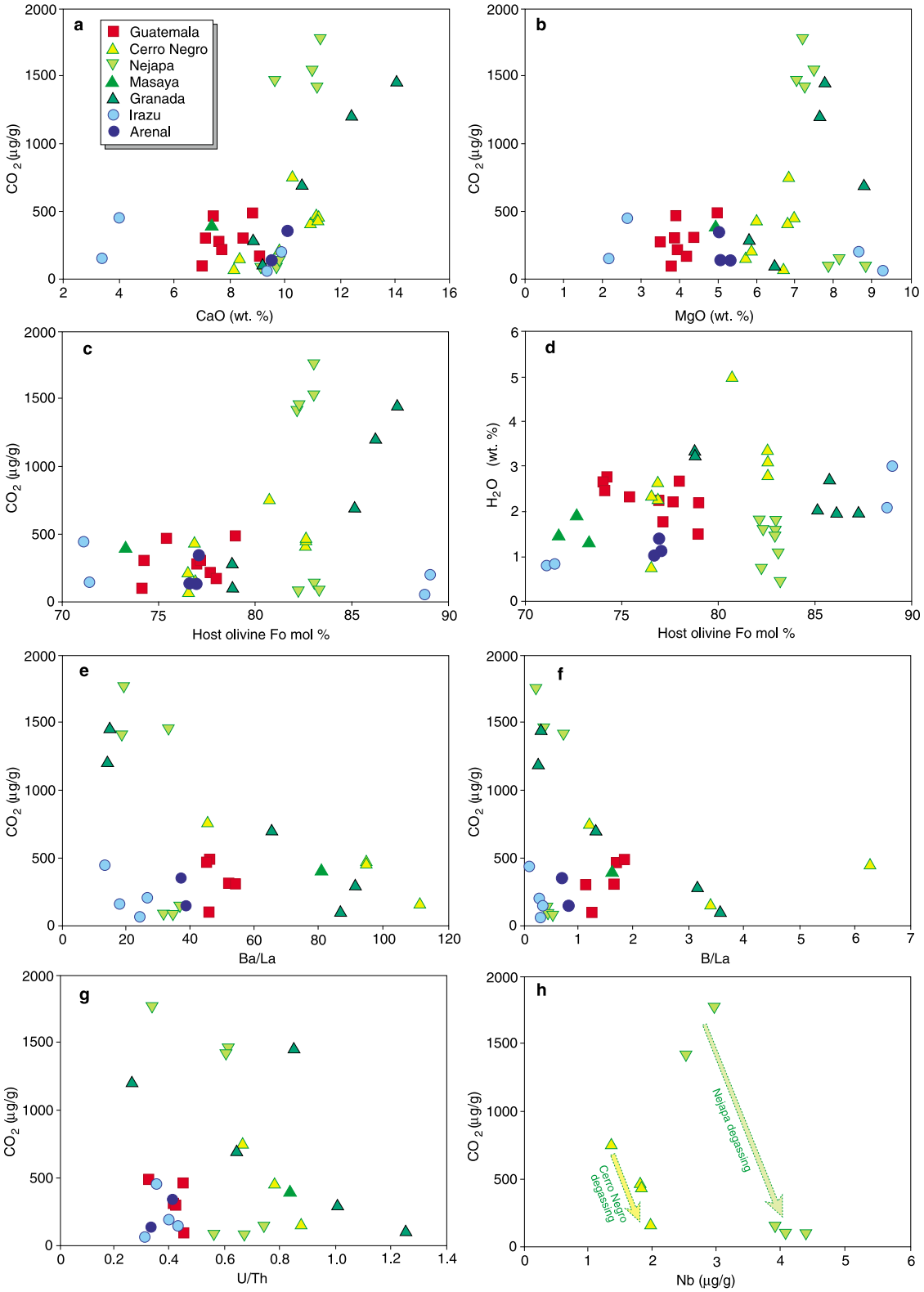

Figure 4. Concentration of CO_2 in melt inclusions plotted versus (a) CaO, (b) MgO, (c) Fo contents of host olivines, (d) concentration of H_2O versus compositions of host olivines, and CO_2 versus (e) Ba/La, (f) B/La, (g) U/Th, (h) Nb. Red squares depict the Guatemalan melt inclusions; the yellow triangles are from Cerro Negro, pale green downward pointing triangles from Nejapa, medium green triangles from Masaya, black-rimmed green triangles from Granada in Nicaragua; dark blue circles from Arenal, light blue circles from Irazú in Costa Rica.

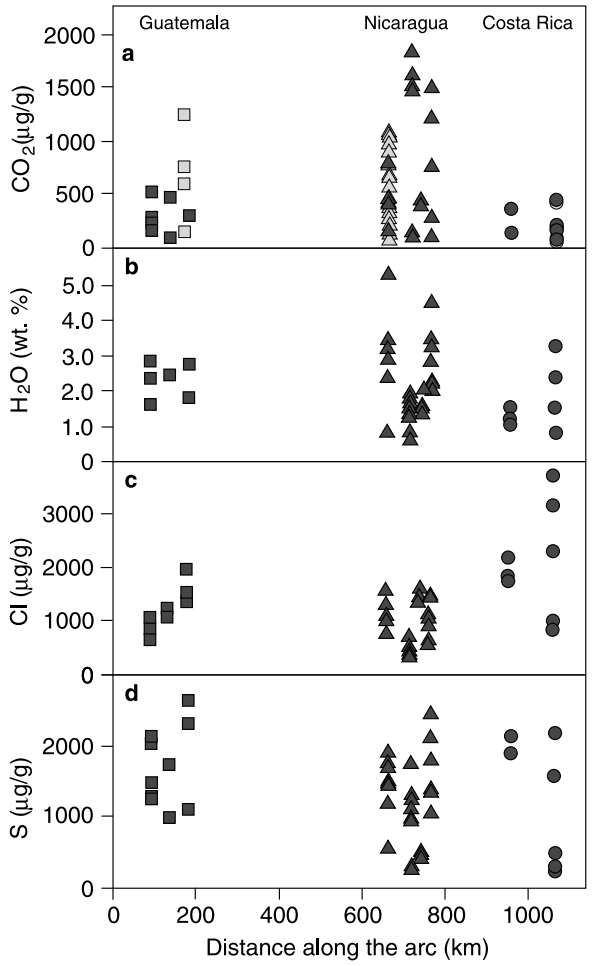

Figure 5. Melt inclusion volatile compositions versus distance along the arc from Guatemala to Costa Rica for (a) CO_2, (b) H_2O, (c) Cl, (d) S; dark gray symbols from this study; light gray symbols show additional data from *Roggensack et al.* [1997] and *Roggensack* [2001a, 2001b] for Guatemala and Nicaragua and from *Wade et al.* [2006] and *Benjamin et al.* [2007] for Costa Rica.

materials were measured repeatedly for additional monitoring of data quality. The instrument's background was monitored by three analyses of an olivine from highly depleted MORB with expected H_2O concentration in olivine below 2 μg/g [*Koga et al.*, 2003]. The background remained at 17–21 μg/g for CO_2, 10–13 μg/g for H_2O, below 1 μg/g for Cl and S.

4. Results

[9] Results for CO_2, H_2O, S, and Cl values are reported in Table 1, corrected for postentrapment crystallization, along with the major and trace element concentrations of the melt inclusions and compositions of the host olivines as published by *Sadofsky et al.* [2008].

[10] CO_2 forms a crude positive correlation with the CaO contents, reaching highest values in the Nicaraguan samples (Figure 4a). In the Granada melt inclusion suite, high CO_2 concentrations (up to 1450 μg/g) are associated with high MgO concentrations (Figure 4b) and forsteritic olivines (Fo > 85; Figure 4c). The Nejapa inclusions form two groups at similarly evolved olivines ($Fo_{83–82}$): a high-CO_2 group with concentrations from 1400 to 1800 μg/g CO_2 and a low-CO_2 group with values in the range of 90–140 μg/g CO_2. In contrast, at Irazú (1963 eruption), a more restricted range of CO_2 concentrations (60–450 μg/g) was measured despite the presence of both very Fo-rich ($Fo_{88–89}$) and fairly evolved (Fo_{71}) olivines (Figure 4c).

[11] Evaluation of along-arc variations is restricted here to a general view because of the limited data set available. The highest CO_2 concentrations were found in Nicaragua (up to 1800 μg/g), while lower concentrations were observed in Costa Rica (60–450 μg/g). The Guatemalan inclusions analyzed in this study range between 100 and 500 μg/g, which is markedly lower than in Nicaragua (Figure 5a). In a previous investigation, however, *Roggensack* [2001a] reported that CO_2 reaches concentrations up to 1249 μg/g at Guatemala's Fuego volcano. Besides CO_2, H_2O concentrations also show peak values in Nicaragua. Whereas H_2O has been shown to correlate with a number of proxies for a slab-derived component [*Wade et al.*, 2006; *Sadofsky et al.*, 2008], CO_2 fails to directly correlate with Ba/La, B/La or U/Th ratios (Figures 4e–4g) and, opposite to H_2O, tends to have the highest concentrations in melt inclusions with the lowest Ba/La, Ba/Th and U/Th ratios (Figures 6a and 6b). The measured Cl concentrations are highest in Costa Rica, but our S data do not show any systematical regional pattern (see Figure 5 and *Sadofsky et al.* [2008]).

5. Discussion

[12] The solubility of CO_2 is very low in silicate magmas, so that in the case of magma saturation it preferentially partitions away from the melt to form a CO_2-bearing fluid phase [e.g., *Dixon et al.*, 1995; *Liu et al.*, 2005; *Papale*, 2005; *Wallace*, 2005; *Papale et al.*, 2006]. Therefore, preentrapment degassing is widely believed to decrease the amount of CO_2 in magmas. Melt inclusions from the CAVA

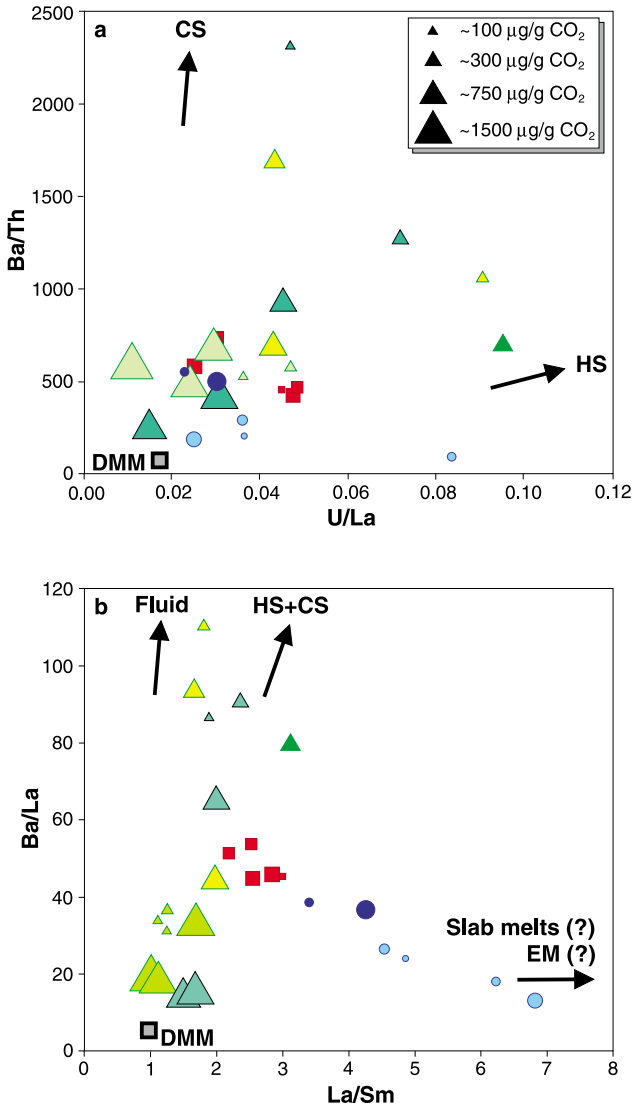

Figure 6. Variations of incompatible trace element ratios in the melt inclusions, modified after *Sadofsky et al.* [2008]. Symbols are as in Figure 4, whereby the sizes of the symbols reflect CO_2 concentrations. (a) Ba/Th versus U/La (weight ratios), showing that the highest CO_2 values occur in samples plotting near mantle compositions, whereas the inclusions with higher sediment contribution show low CO_2. Compositions of carbonate and hemipelagic sediments (CS and HS, respectively) are from DSDP site 495 [*Patino et al.*, 2000]; DMM denotes depleted MORB mantle source after *Salters and Stracke* [2004]. (b) Ba/La versus La/Sm, underscoring the lower CO_2 concentrations at increasing fluid/sediment or slab melt input [after *Sadofsky et al.*, 2008]. Again, samples plotting close to mantle values (DMM) have the highest CO_2 concentrations.

rocks studied here are hosted in olivines of variable and mostly evolved compositions, and thus are expected to represent variably degassed magmas. When CO_2 concentrations from a particular locality decrease with for example decreasing Fo contents of the host olivines (Figure 4c), along with an increase in incompatible elements, magmatic degassing as magma differentiation proceeded appears to be the major process affecting CO_2 concentrations in the melt inclusions. This is observed here at Nejapa, and to a lesser extent at Cerro Negro (Nicaragua) (Figure 4h). An additional process which is known to deplete CO_2 in the residual melt in inclusions is the formation of bubbles [*Métrich and Wallace*, 2008]. Although the effect of this process cannot be quantitatively accounted for at present, it is similar to magmatic degassing and drives the melt composition toward lower CO_2 contents at nearly constant or slightly decreasing H_2O.

[13] Because concentrations of CO_2 in the glasses of many inclusions studied here were likely compromised by bubble formation, it is only possible to infer the minimum pressures at the time of melt inclusion entrapment. The pressures were estimated here by using two alternative models for the solubility of mixed CO_2-H_2O fluids in magmas, which are VolatileCalc [*Newman and Lowenstern*, 2002] (Figures 7a and 7b) and the model of *Papale et al.* [2006] (Figures 8a–8d). Even though the models were revealed to have some intrinsic restrictions when applied to arc magmatism [e.g., *Burton et al.*, 2007; *Moore*, 2008; *Roggensack and Moore*, 2009; *Johnson et al.*, 2010], they appear to bracket the possible pressure range at given H_2O and CO_2 contents in island arc melts as shown in recent work by *Shishkina et al.* [2010]. Based on the available data, the VolatileCalc model allows us to reconstruct the minimum pressure range of melt saturation with a CO_2-H_2O fluid to range from 370 to 25 MPa for Nejapa and Cerro Negro melts (Figure 7a). The melt inclusions from Granada, Irazú, and Santa María indicate a narrower pressure range, generally not exceeding 130 MPa (Figure 7b).

[14] The low H_2O contents previously reported in some of the Central American subduction-related volcanic rocks and particularly from Nicaragua [*Sadofsky et al.*, 2008] could reflect preentrapment H_2O degassing at low pressures. The high CO_2 contents and steep degassing curve for samples with relatively low H_2O (1.6–1.9 wt. %) at Nejapa, however, indicate that these low H_2O contents are features of the parental melt (Figure 7a). Inclusions from Cerro Negro are collectively considered here from the 1971, 1992, and 1999 eruptions and complemented by literature data from the 1992 and 1995 eruptions [*Roggensack et al.*, 1997] to delineate the degassing trend of the young magmatic system. At Cerro Negro, melt inclusion chemistry correlates with host crystal size and thus melts were interpreted to evolve and decompress in a shallow ephemeral dike system (sub-) continuously fed by a deeper source, implying that multiple magmas have interacted in individual eruptions [*Roggensack*, 2001b]. Compared to Nejapa, the Cerro Negro melt inclusions fall along a shallower trend (Figure 7a), which would imply either an unrealistically large amount of fluid phase in the magma during closed system degassing, or, more likely, result from open system addition of a CO_2-rich gas phase. Such gas fluxing into the rising magma from below would induce a lowering of the melt water content as the system strives for reequilibration with the gas phase [*Métrich and Wallace*, 2008; *Johnson et al.*, 2010]. The gas phase might be released from degassing deeper magma [*Johnson et al.*, 2010] or from a slab fluid that was never part of a melt. *Métrich and Wallace* [2008] conclude that such gas fluxing processes may be a common feature in basaltic systems.

[15] The crudely inverse trend on the H_2O versus CO_2 diagram for the Santa María suite and the melt inclusions from the 1963 Irazú eruption indicate that these melt inclusions could have been trapped during isobaric magma fractionation at fluid-saturated conditions leading to an enrichment of the melt in H_2O and depletion in CO_2 (Figure 7b). Isobaric trends inferred for melts from long-living volcanoes such as Santa María and Irazú would be consistent with the possible presence of shallow magma chambers beneath these volcanoes. This contrasts with the findings of *Benjamin et al.* [2007], who reconstructed a rather simple path of degassing coupled with crystallization as the magma ascended prior to the 1723 Irazú eruption.

[16] At Granada, inclusions show a negative correlation between Fo content of the olivine and the H_2O content of the melt inclusion, which could reflect incompatible behavior of water during differentiation (Figure 4d). This would imply that the low water contents more closely reflect the composition of the undegassed parental magmas. The relationship between H_2O and CO_2, however, indicates that these melts do not follow any simple degassing path at polybaric or isobaric conditions and therefore were likely derived from two distinct parental magmas with high and low H_2O contents. This is consistent with the interpretation of *Sadofsky et al.* [2008], who also pointed to strikingly different trace element patterns of the high- and low-H_2O Granada

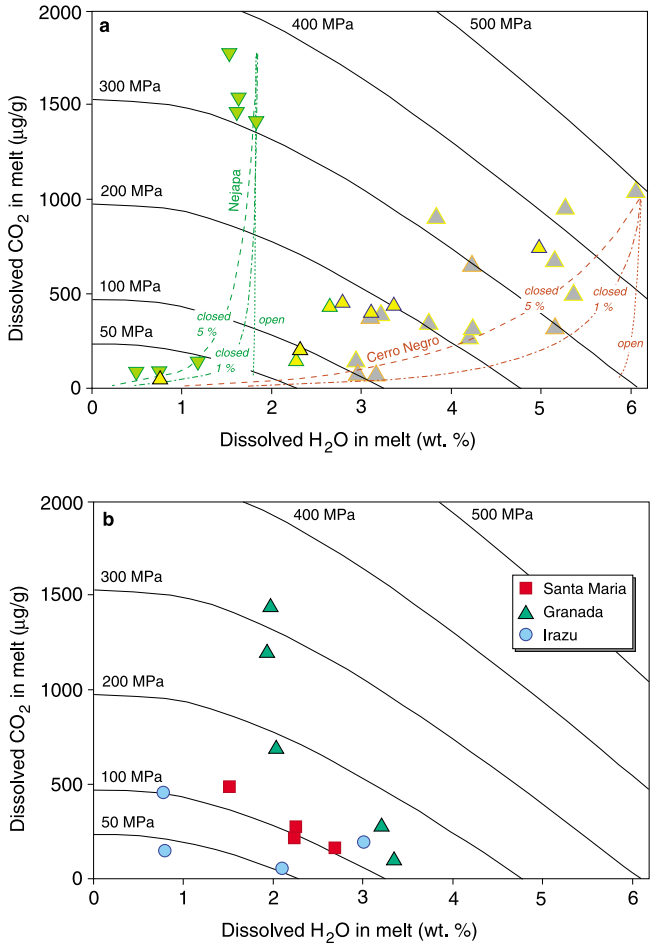

Figure 7. (a) CO_2 versus H_2O for Nejapa (inverted green triangles) and Cerro Negro melt inclusions (this study: yellow triangles with blue rims for 1971 eruption, with black rims for 1992 eruption, with green rims for 1999 eruption; data from *Roggensack et al.* [1997]: gray triangles with yellow rims for 1992 eruption, with orange rims for 1995 eruption). Melt inclusions from the 1992 eruptions analyzed in this study are considerably more degassed than those presented by *Roggensack et al.* [1997]. Formation of gas bubbles in the melt inclusions after entrapment might reduce volatile concentrations in the glass by gas redistribution from the silicate melt toward the bubble during the cooling process, thus representing minimum concentration values as well as minimum saturation pressures [*Métrich and Wallace*, 2008]. Saturation isobars are shown for pressures of 50 to 500 MPa. Degassing paths were modeled using VolatileCalc 1.1 [*Newman and Lowenstern*, 2002] at temperatures of 1200°C for Nejapa and 1160°C for Cerro Negro (estimated from mineral-melt phase equilibria); dotted lines indicate open system degassing, while dash-dotted lines represent closed system degassing with 1% exsolved vapor assumed, and dashed lines represent closed system degassing with 5% exsolved vapor assumed. Nejapa melt inclusions follow a low-degree closed system degassing trend. For the Cerro Negro system, melt inclusions depart from the predicted degassing trends, which is likely related to an open system gas fluxing process [*Métrich and Wallace*, 2008]. For Nejapa, CO_2 degassed over the same pressure interval without significant loss of H_2O, underlining the much lower solubility of CO_2 in silicate melts compared to H_2O, which essentially remained dissolved till about 50 MPa. (b) CO_2 versus H_2O for Granada (black-rimmed green triangles), Irazú (light blue circles), and Santa María (red squares) melt inclusions. Entrapment at narrower ranges of saturation pressures indicates more limited degassing than observed at Nejapa and Cerro Negro.

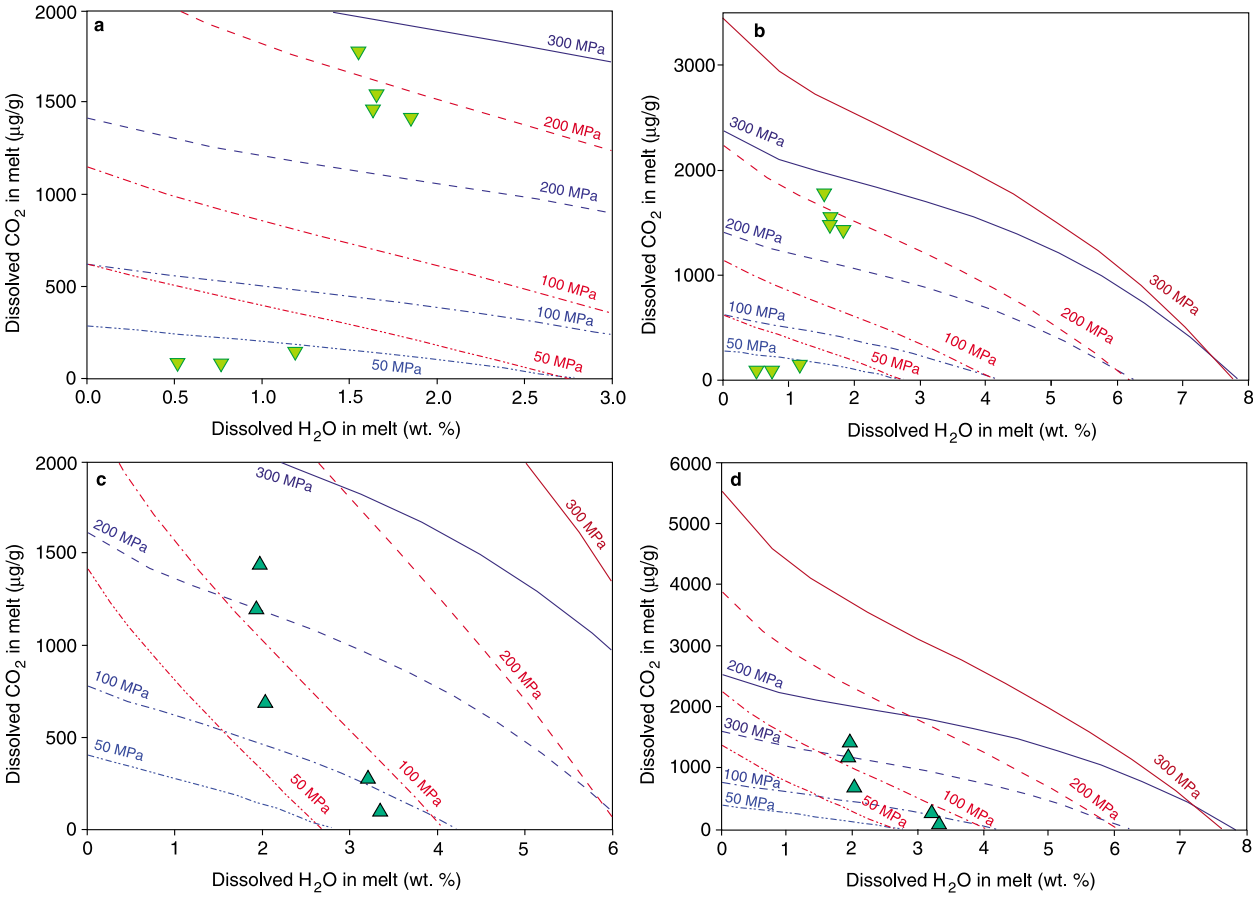

Figure 8. Plots of melt inclusion CO_2 versus H_2O concentrations for (a and b) Nejapa (Figure 8a is a close-up of Figure 8b) and (c and d) Granada (Figure 8c is a close-up of Figure 8d), including saturation isobars based on the model of *Papale et al.* [2006]. Red lines depict saturation isobars calculated with an average of the high-CO_2, high-CaO group of Nejapa, and the highest-CO_2, highest CaO inclusion of Granada, respectively. Blue lines show saturation isobars of the averaged low-CO_2, low-CaO Nejapa inclusions, and the lowest CO_2, second lowest CaO inclusion of Granada. Temperature assumptions were 1189°C for Nejapa (high), 1232°C for Nejapa (low), 1451°C for Granada (high), and 1174°C for Granada (low), based on mineral-melt equilibria. The differences between the corresponding isobars illustrate the effect of decreasing CaO on decreasing the solubility of CO_2 as predicted by the *Papale et al.* [2006] model. The modeled saturation pressures are lower than those estimated with VolatileCalc (Figures 7a and 7b). For further discussion how these models compare, see also *Shishkina et al.* [2010].

melts, the former being an arc-type low-Nb melt, carrying a carbonate sediment signature, and the latter being a high-Nb melt, derived from an E-MORB-type mantle wedge composition with only minor contribution from the subducting slab.

[17] Diagrams of Ba/Th versus U/La, or Ba/La versus La/Sm (Figures 6a and 6b) can be used to assess the contributions of hemipelagic and carbonate sediments to the mantle wedge [*Patino et al.*, 2000]. Interestingly, the inferred subducted sediment contribution and CO_2 content in melt inclusions appear to be decoupled. The highest CO_2, though lowest H_2O contents are observed in samples with the most depleted (MORB-like) trace element compositions. While MORB-like inclusions with low CO_2 are also present, none of the strongly slab-affected inclusions show a significant CO_2 enrichment (Figures 6a and 6b).

[18] A comparison of CO_2 with Nb can be instructive (Figure 9), since both are highly incompatible and have similar partition coefficients during mantle melting. The CO_2/Nb ratio in primitive MORB shows a relatively large range with proposed values of 239 [*Saal et al.*, 2002] and ~530 [*Cartigny et al.*, 2008], and an average value of ~400 [*Hauri and Saal*, 2009]. The least degassed melt inclusions studied here have CO_2/Nb values similar to those of MORB, which is best expressed in the Granada melt inclusion suite. This suggests that the observed CO_2

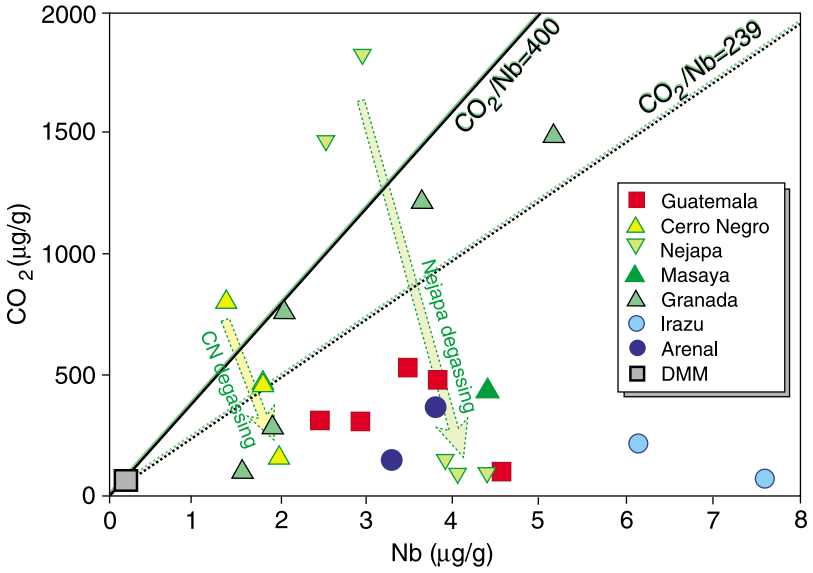

Figure 9. Melt inclusion CO_2 versus Nb concentrations, symbols are as in Figure 4. Green-shaded black lines show the MORB CO_2/Nb ratios of 400 after *Hauri and Saal* [2009] and of 239 after *Saal et al.* [2002], DMM denotes depleted MORB mantle source after *Salters and Stracke* [2004]. The samples with the highest CO_2 have CO_2/Nb ratios similar to MORB.

concentrations in the melt inclusions were derived primarily from the mantle wedge.

6. CO_2 Output Rate Quantification

[19] Although our data on partially degassed melt inclusions cannot provide information about the total CO_2 fluxes from CAVA volcanism, the high-CO_2 melt inclusions that have E-MORB-like compositions yield information on the CO_2 flux from the mantle wedge to the surface with only a limited overprint from the slab. Details concerning our output rate calculation are provided Text S1 and Table S2 in the auxiliary material. These calculations indicate an arc-length-normalized output of 2.6×10^{-2} g/m/s CO_2, equivalent to a rate of 2.8×10^4 g/s for the entire arc (~1100 km). As expected, this rate estimate is lower than those reported in previous studies for the entire CO_2 flux through the subduction system. *Hilton et al.* [2002] estimated 8.1×10^4 g/s output flux of CO_2 for the entire CAVA (unit converted from 6.9×10^{11} g C per year) by COSPEC remote sensing techniques coupled with measured SO_2-CO_2 gas ratios. This estimate is slightly lower than the value of 9.9×10^4 g/s (unit converted from 7.1×10^{10} mol CO_2 per year) of *Shaw et al.* [2003] obtained from C-He gas ratios characterizing quiescent degassing. Numerical modeling by *Gorman et al.* [2006] produced CAVA subarc CO_2 fluxes of 9.2×10^4 g/s (6.6×10^{10} mol/year), in agreement with the results of *Hilton et al.* [2002] and *Shaw et al.* [2003] but about three times higher than our estimated output rate from the mantle wedge.

[20] For two reasons, however, it should not be attempted to reconcile these flux estimates derived from approaches of such strongly different nature with an expectation of conformity in absolute values. First, the CO_2 emission from open vents is usually monitored over periods of seconds to a few years, hence potentially capturing features of short-term variability [e.g., *Garofalo et al.*, 2007], while the melt inclusions investigated in this study cover time spans of years to tens of ka at a lower temporal resolution. Likewise, reference values when flux estimates are based on gas ratios may be subject to temporal or geographic variability. This might apply for example for ^{3}He output fluxes, which were in previous studies adopted from published values for mid-ocean ridge degassing, and assumed to be representative for global arc mantle wedges.

[21] Second, and more important, the differences in the estimated fluxes reflect different processes in the subduction system. Studies of quiescent degassing are more likely to quantify the total amount of CO_2 released from melts, including those that remain as intrusions solidified in the lithosphere and from the fractions of CO_2 in the erupting magmas that exsolve to form free CO_2-bearing fluid phases. As inferred from the low CO_2 concentrations in the melt

inclusions with the highest slab signal, this latter process appears to be most pronounced in melts with the highest contribution of CO_2 from the subducting plate, derived primarily from the subducted sediments and carbonate in the crust. In contrast, the highest concentrations of CO_2 in the melt inclusions can be well accounted for by mantle melting without significant contribution from subducting slab. The difference between the flux estimates can therefore serve to distinguish between the CO_2 flux from the mantle wedge, represented by the highest-CO_2 MORB-like melt inclusions, and the total flux from the subduction system, derived from quiescent degassing and numerical modeling. Our results, combined with the published fluxes, therefore imply that about two thirds of the CO_2 emitted from the entire Central American subduction system originated from the subducting slab. This ratio implies a higher mantle contribution to the total budget of CO_2 than previous estimates, which provide percentages of 10% mantle origin, while 76% are considered to stem from marine carbonates and 14% from organic sediments [*de Leeuw et al.*, 2007]. The estimate of *Shaw et al.* [2003] attributes an even higher portion to the marine carbonates (86.4% relative to 5.6% mantle and 8.1% organic sediments). With regard to atmospheric effects of arc volcanism, this means that explosive CO_2 emissions into higher atmospheric levels involve only a subordinate fraction of the total CO_2 emitted. A far larger amount of CO_2 reaches the surface through quiescent degassing and is discharged into the atmosphere at near-surface altitudes.

7. Conclusions

[22] Olivine-hosted melt inclusions from the mafic tephras along the CAVA analyzed in this study contain up to 450 μg/g in Costa Rica, 1800 μg/g in Nicaragua, and 500 μg/g CO_2 in Guatemala. The highest CO_2 concentrations are found in the inclusions that trend toward MORB-like compositions. CO_2 contents are decoupled from geochemical slab tracers such as Ba/La, Ba/Th, and U/La, suggesting that either the large input of sediments and carbonated slab components at the CAVA does not inherently lead to an increased CO_2 output signal, or that stronger degassing takes place in the most slab-affected melts because of an early formation of a CO_2-bearing fluid phase. CO_2/Nb ratios in the least degassed melt inclusions from small cinder cones such as Granada and Nejapa are within the MORB array and suggest that the CO_2 in these inclusions could be close to that in undegassed melts formed from the mantle wedge. The CO_2 emissions estimated for the mantle wedge amounts to 2.8×10^4 g/s. Comparison of this rate with published data derived from both quiescent degassing and numerical modeling, which are more likely to represent a total CO_2 flux for the subduction system, implies that two thirds of the CO_2 flux to the surface in Central America is derived from the subducting plate. This study indicates that the CO_2 in melt inclusions can only provide minimal flux of CO_2 out of a volcanic arc. The power of volatile contents in melt inclusions, however, is that combined with the major and trace element composition of the inclusion, they can help identify a range of parental melt compositions and distinguish different processes in magmatic systems such as polybaric or isobaric fractionation and also identify gas fluxing from depth.

Acknowledgments

[23] We are grateful to Paul Wallace and an anonymous reviewer for their detailed and helpful comments that improved this manuscript. Seth Sadofsky and Paul van den Bogaard participated in sample collection and preparation. Staff members of Central American Geologic Services INETER, ICE, SNET, and INSIVUMEH were of great help with the field logistics. Igor Nikogosian and Roman Botcharnikov are thanked for providing reference glasses for the CO_2 measurements. Credit is due to Mark Ghiorso for providing the possibility to use the solubility model of *Papale et al.* [2006] through the OFM Research webpage. This paper is contribution 143 to Sonderforschungsbereich 574 "Volatiles and fluids in subduction zones" at Kiel University, funded by the German Research Foundation.

References

Auger, L. S., G. Abers, K. Fisher, M. Protti, V. Gonzales, and W. Strauch (2006), Crustal thickness variations beneath the Central American Volcanic Arc, *Eos Trans. AGU*, *87*(52), Fall Meet. Suppl., Abstract T23C-0517.

Benjamin, E. R., T. Plank, J. A. Wade, K. A. Kelley, E. H. Hauri, and G. E. Alvarado (2007), High water contents in basaltic magmas from Irazú Volcano, Costa Rica, *J. Volcanol. Geotherm. Res.*, *168*, 68–92, doi:10.1016/j.jvolgeores.2007.08.008.

Burton, M., P. Allard, F. Muré, and A. La Spina (2007), Magmatic gas composition reveals the source depth of slug-driven Strombolian explosive activity, *Science*, *317*, 227–230, doi:10.1126/science.1141900.

Carr, M. J., M. D. Feigenson, and E. A. Bennett (1990), Incompatible element and isotopic evidence for tectonic control of source mixing and melt extraction along the Central American Volcanic Arc, *Contrib. Mineral. Petrol.*, *105*, 369–380, doi:10.1007/BF00286825.

Cartigny, P., F. Pineau, C. Aubaud, and M. Javoy (2008), Towards a consistent mantle carbon flux estimate: Insights from volatile systematics (H_2O/Ce, δD, CO_2/Nb) in the

North Atlantic mantle (14°N and 34°N), *Earth Planet. Sci. Lett.*, *265*, 672–685, doi:10.1016/j.epsl.2007.11.011.

Connolly, J. A. D. (2005), Computation of phase equilibria by linear programming: A tool for geodynamic modeling and its application to subduction zone decarbonation, *Earth Planet. Sci. Lett.*, *236*, 524–541, doi:10.1016/j.epsl.2005.04.033.

Danyushevsky, L. V., S. M. Eggins, T. J. Falloon, and D. M. Christie (2000), H_2O abundance in depleted to moderately enriched mid-ocean ridge magmas. Part I: Incompatible behaviour, implications for mantle storage, and origin of regional variations, *J. Petrol.*, *41*, 1329–1364, doi:10.1093/petrology/41.8.1329.

de Leeuw, G. A. M., D. R. Hilton, T. P. Fischer, and J. A. Walker (2007), The He-CO_2 isotope and relative abundance characteristics of geothermal fluids in El Salvador and Honduras: New constraints on volatile mass balance of the Central American Volcanic Arc, *Earth Planet. Sci. Lett.*, *258*, 132–146, doi:10.1016/j.epsl.2007.03.028.

DeMets, C. (2001), A new estimate for present-day Cocos-Caribbean Plate motion: Implications for slip along the Central American Volcanic Arc, *Geophys. Res. Lett.*, *28*, 4043–4046, doi:10.1029/2001GL013518.

Dixon, J. E. (1997), Degassing of alkalic basalts, *Am. Mineral.*, *82*, 368–378.

Dixon, J. E., E. M. Stolper, and J. M. Holloway (1995), An experimental study of water and carbon dioxide solubilities in mid-ocean ridge basaltic liquids. Part I: Calibration and solubility models, *J. Petrol.*, *36*, 1607–1631.

Fryer, P., C. G. Wheat, and M. J. Mottl (1999), Mariana blueschist mud volcanism: Implications for conditions within the subduction zone, *Geology*, *27*, 103–106, doi:10.1130/0091-7613(1999)027<0103:MBMVIF>2.3.CO;2.

Garofalo, K., F. Tassi, O. Vaselli, A. Delgado-Huertas, D. Tedesco, M. Frische, T. H. Hansteen, R. J. Poreda, and W. Strauch (2007), Fumarolic gases at Mombacho volcano (Nicaragua): Presence of magmatic gas species and implications for volcanic surveillance, *Bull. Volcanol.*, *69*, 785–795, doi:10.1007/s00445-006-0108-z.

Gazel, E., M. J. Carr, K. Hoernle, M. D. Feigenson, D. Szymanski, F. Hauff, and P. van den Bogaard (2009), Galapagos-OIB signature in southern Central America: Mantle refertilization by arc-hot spot interaction, *Geochem. Geophys. Geosyst.*, *10*, Q02S11, doi:10.1029/2008GC002246.

Gorman, P. J., D. M. Kerrick, and J. A. D. Connolly (2006), Modeling open system metamorphic decarbonation of subducting slabs, *Geochem. Geophys. Geosyst.*, *7*, Q04007, doi:10.1029/2005GC001125.

Grevemeyer, I., C. R. Ranero, E. R. Flueh, D. Klaeschen, and J. Bialas (2007), Passive and active seismological study of bending-related faulting and mantle serpentinization at the Middle America trench, *Earth Planet. Sci. Lett.*, *258*, 528–542, doi:10.1016/j.epsl.2007.04.013.

Hauri, E. H., and A. E. Saal (2009), Volatile element variability in MORB: Origins and consequences, *Geochim. Cosmochim. Acta*, *73*, Suppl. 1, Abstract A503, doi:10.1016/j.gca.2009.05.006.

Hauri, E. H., J. Wang, J. E. Dixon, P. L. King, C. Mandeville, and S. Newman (2002), SIMS analysis of volatiles in silicate glasses 1. Calibration, matrix effects and comparison with FTIR, *Chem. Geol.*, *183*, 99–114, doi:10.1016/S0009-2541(01)00375-8.

Hilton, D. R., T. P. Fischer, and B. Marty (2002), Noble gases and volatile recycling at subduction zones, *Rev. Mineral. Geochem.*, *47*, 319–370, doi:10.2138/rmg.2002.47.9.

Hoernle, K., R. Werner, J. P. Morgan, D. Garbe-Schönberg, J. Bryce, and J. Mrazek (2000), Existence of complex spatial zoning in the Galapagos Plume, *Geology*, *28*, 435–438, doi:10.1130/0091-7613(2000)28<435:EOCSZI>2.0.CO;2.

Hoernle, K., G. Tilton, M. J. Le Bas, S. Duggen, and D. Garbe-Schönberg (2002), Geochemistry of oceanic carbonatites compared with continental carbonatites: Mantle recycling of oceanic crustal carbonate, *Contrib. Mineral. Petrol.*, *142*, 520–542, doi:10.1007/s004100100308.

Hoernle, K., D. L. Abt, K. M. Fischer, H. Nichols, F. Hauff, G. Abers, P. van den Bogaard, G. Alvarado, J. M. Protti, and W. Strauch (2008), Geochemical and geophysical evidence for arc-parallel flow in the mantle wedge beneath Costa Rica and Nicaragua, *Nature*, *451*, 1094–1097, doi:10.1038/nature06550.

Ivandic, M., I. Grevemeyer, A. Berhorst, E. R. Flueh, and K. McIntosh (2008), Impact of bending related faulting on the seismic properties of the incoming oceanic plate offshore of Nicaragua, *J. Geophys. Res.*, *113*, B05410, doi:10.1029/2007JB005291.

Johnson, E. R., P. J. Wallace, K. V. Cashman, and H. Delgado Granados (2010), Degassing of volatiles (H_2O, CO_2, S, Cl) during ascent, crystallization, and eruption at mafic monogenetic volcanoes in central Mexico, *J. Volcanol. Geotherm. Res.*, *197*, 225–238, doi:10.1016/j.jvolgeores.2010.02.017.

Koga, K., E. H. Hauri, M. Hirschmann, and D. Bell (2003), Hydrogen concentration analyses using SIMS and FTIR: Comparison and calibration for nominally anhydrous minerals, *Geochem. Geophys. Geosyst.*, *4*(2), 1019, doi:10.1029/2002GC000378.

Kulm, L. D., and E. Suess (1990), Relationship between carbonate deposits and fluid venting: Oregon accretionary prism, *J. Geophys. Res.*, *95*, 8899–8915, doi:10.1029/JB095iB06p08899.

Ligorria, J. P., and E. Molina (1997), Crustal velocity structure of Southern Guatemala using refracted and SP converted waves, *Geofis. Int.*, *36*, 9–19.

Liu, Y., Y. Zhang, and H. Behrens (2005), Solubility of water in rhyolitic melts at low pressures and a new empirical model for mixed H_2O+CO_2 solubility in rhyolitic melts, *J. Volcanol. Geotherm. Res.*, *143*, 219–235, doi:10.1016/j.jvolgeores.2004.09.019.

MacKenzie, L., G. A. Abers, K. M. Fisher, E. M. Syracuse, J. M. Protti, V. Gonzales, and W. Strauch (2008), Crustal structure along the southern Central American volcanic front, *Geochem. Geophys. Geosyst.*, *9*, Q08S09, doi:10.1029/2008GC001991.

Métrich, N., and P. Wallace (2008), Volatile abundance in basaltic magmas and their degassing paths tracked by melt inclusions, *Rev. Mineral. Geochem.*, *69*, 363–402, doi:10.2138/rmg.2008.69.10.

Moore, G. (2008), Interpreting H_2O and CO_2 contents in melt inclusions: Constraints from solubility experiments and modeling, *Rev. Mineral. Geochem.*, *69*, 333–362, doi:10.2138/rmg.2008.69.9.

Narcía-López, C., R. R. Castro, and C. J. Rebollar (2004), Determination of crustal thickness beneath Chiapas, Mexico using S and Sp waves, *Geophys. J. Int.*, *157*, 215–228, doi:10.1111/j.1365-246X.2004.02173.x.

Newman, S., and J. B. Lowenstern (2002), VolatileCalc: A silicate-melt-H_2O-CO_2 solution model written in Visual Basic for Excel, *Comput. Geosci.*, *28*, 597–604, doi:10.1016/S0098-3004(01)00081-4.

Papale, P. (2005), Determination of total H_2O and CO_2 budgets in evolving magmas from melt inclusion data, *J. Geophys. Res.*, *110*, B03208, doi:10.1029/2004JB003033.

Papale, P., R. Moretti, and D. Barbato (2006), The compositional dependence of the saturation surface of H_2O+CO_2 in fluids in silicate melts, *Chem. Geol.*, *229*, 78–95, doi:10.1016/j.chemgeo.2006.01.013.

Patino, L. C., M. J. Carr, and M. D. Feigenson (2000), Local and regional variations in Central American arc lavas controlled by variations in subducted sediment input, *Contrib. Mineral. Petrol.*, *138*, 265–283, doi:10.1007/s004100050562.

Plank, T., V. Balzer, and M. Carr (2002), Nicaraguan volcanoes record paleoceanographic changes accompanying closure of the Panama gateway, *Geology*, *30*, 1087–1090, doi:10.1130/0091-7613(2002)030<1087:NVRPCA>2.0.CO;2.

Ranero, C. R., J. Phipps Morgan, K. McIntosh, and C. Reichert (2003), Bending, faulting, and mantle serpentinization at the Middle America Trench, *Nature*, *425*, 367–373, doi:10.1038/nature01961.

Roggensack, K. (2001a), Unraveling the 1974 eruption of Fuego volcano (Guatemala) with small crystals and their young melt inclusions, *Geology*, *29*, 911–914, doi:10.1130/0091-7613(2001)029<0911:UTEOFV>2.0.CO;2.

Roggensack, K. (2001b), Sizing up crystals and their melt inclusions: A new approach to crystallization studies, *Earth Planet. Sci. Lett.*, *187*, 221–237, doi:10.1016/S0012-821X(01)00269-2.

Roggensack, K., and G. M. Moore (2009), New constraints for fluid compositions of melt inclusions: Results from H_2O and CO_2 solubility experiments at 200 to 400 MPa, *Eos Trans. AGU*, *90*(52), Fall Meet. Suppl., Abstract V23H-01.

Roggensack, K., R. L. Hervig, S. B. McKnight, and S. N. Williams (1997), Explosive basaltic volcanism from Cerro Negro: Influence of volatiles on eruptive style, *Science*, *277*, 1639–1642, doi:10.1126/science.277.5332.1639.

Saal, A. E. M., E. H. Hauri, C. H. Langmuir, and M. R. Perfitt (2002), Vapour undersaturation in primitive mid-ocean-ridge basalt and the volatile content of Earth's upper mantle, *Nature*, *419*, 451–455, doi:10.1038/nature01073.

Sadofsky, S. J., M. V. Portnyagin, K. Hoernle, and P. van den Bogaard (2008), Subduction cycling of volatile and trace elements through the Central American Volcanic Arc: Evidence from melt inclusions, *Contrib. Mineral. Petrol.*, *155*, 433–456, doi:10.1007/s00410-007-0251-3.

Sadofsky, S. J., K. Hoernle, S. Duggen, F. Hauff, and R. Werner (2009), Geochemical variations in the Cocos Plate subducting offshore of Central America, *Int. J. Earth Sci.*, *98*, 901–913, doi:10.1007/s00531-007-0289-5.

Salters, V. J. M., and A. Stracke (2004), Composition of the depleted mantle, *Geochem. Geophys. Geosyst.*, *5*, Q05B07, doi:10.1029/2003GC000597.

Shaw, A. M., D. R. Hilton, T. P. Fischer, J. A. Walker, and G. E. Alvarado (2003), Contrasting He-C relationships in Nicaragua and Costa Rica: Insights into C cycling through subduction zones, *Earth Planet. Sci. Lett.*, *214*, 499–513, doi:10.1016/S0012-821X(03)00401-1.

Shaw, A. M., D. R. Hilton, T. P. Fischer, and E. H. Hauri (2007), Volatile fluxes at arc volcanoes: Comparing different techniques and evaluating mass balances. Abstract, SubFac SEIZE meeting, Heredia, Costa Rica, June 18–22, 2007.

Shishkina, T. A., R. E. Botcharnikov, F. Holtz, R. R. Almeev, and M. V. Portnyagin (2010), Solubility of H_2O- and CO_2-bearing fluids in tholeiitic basalts at pressures up to 500 MPa, *Chem. Geol.*, *277*, 115–125, doi:10.1016/j.chemgeo.2010.07.014.

Snyder, G., R. Poreda, A. Hunt, and U. Fehn (2001), Regional variations in volatile composition: Isotopic evidence for carbonate recycling in the Central American Volcanic Arc, *Geochem. Geophys. Geosyst.*, *2*, 1057, doi:10.1029/2001GC000163.

Sobolev, A. V., and M. Chaussidon (1996), H_2O concentrations in primary melts from supra-subduction zones and mid-ocean ridges: Implications for H_2O storage and recycling in the mantle, *Earth Planet. Sci. Lett.*, *137*, 45–55, doi:10.1016/0012-821X(95)00203-O.

Syracuse, E. M., and G. A. Abers (2006), Global compilation of variations in slab depth beneath arc volcanoes and implications, *Geochem. Geophys. Geosyst.*, *7*, Q05017, doi:10.1029/2005GC001045.

Tera, F., L. Brown, J. Morris, I. S. Sacks, J. Klein, and R. Middleton (1986), Sediment incorporation in island-arc magmas: Inferences from ^{10}Be, *Geochim. Cosmochim. Acta*, *50*, 535–550, doi:10.1016/0016-7037(86)90103-1.

Wade, J. A., T. Plank, W. G. Melson, G. J. Soto, and E. H. Hauri (2006), The volatile content of magmas from Arenal volcano, Costa Rica, *J. Volcanol. Geotherm. Res.*, *157*, 94–120, doi:10.1016/j.jvolgeores.2006.03.045.

Walker, J. A., K. Roggensack, L. C. Patino, B. Cameron, and O. Matias (2003), The water and trace element contents of melt inclusions across an active subduction zone, *Contrib. Mineral. Petrol.*, *146*, 62–77, doi:10.1007/s00410-003-0482-x.

Wallace, P. J. (2005), Volatiles in subduction zone magmas: Concentrations and fluxes based on melt inclusions and volcanic gas data, *J. Volcanol. Geotherm. Res.*, *140*, 217–240, doi:10.1016/j.jvolgeores.2004.07.023.

Werner, R., K. Hoernle, P. van den Bogaard, C. Ranero, R. von Huene, and D. Korich (1999), Drowned 14-m.y.-old Galapagos Archipelago off the coast of Costa Rica; implications for tectonic and evolutionary models, *Geology*, *27*, 499–502, doi:10.1130/0091-7613(1999)027<0499:DMYOGP>2.3.CO;2.

Werner, R., K. Hoernle, U. Barckhausen, and F. Hauff (2003), Geodynamic evolution of the Galápagos hot spot system (central east Pacific) over the past 20 m.y.: Constraints from morphology, geochemistry, and magnetic anomalies, *Geochem. Geophys. Geosyst.*, *4*(12), 1108, doi:10.1029/2003GC000576.